JOURNAL OF SPACECRAFT AND ROCKETS
Vol. 35, No. 5, September–October 1998

Three-Dimensional Flow Computation Around a Projectile Overtaking a Preceding Shock Wave

Rikio Watanabe*
Tokyo Noko University, Tokyo 184, Japan
Kozo Fujii†
Institute of Space and Astronautical Science, Kanagawa 229, Japan
and
Fumio Higashino‡
Tokyo Noko University, Tokyo 184, Japan

A numerical simulation of the flowfield around a projectile overtaking a preceding shock wave is carried out by solving the three-dimensional, thin-layer Navier–Stokes equations. A domain decomposition method with the fortified solution algorithm interface scheme is used to supply reasonable grid configurations for such an unsteady flowfield. Computed results show that complicated interaction flowfields are observed while overtaking the shock wave. The results of the two- and three-dimensional flowfield computations are compared, and the characteristic features of the three-dimensional flowfield are shown. Time histories of the aerodynamic forces show that the projectile suffers strong asymmetric forces while overtaking the shock wave, which may make the trajectory of the projectile unstable.

Nomenclature

C_D = drag coefficient, $[D/(1/2\rho_0 U_p^2 S_b)]$
C_{my}, C_{mz} = moment coefficients around x and y axes
C_p = pressure coefficient, $[(p - p_0)/(1/2\rho_0 U_p^2)]$
C_y, C_z = lateral force coefficients
c_0 = speed of sound in the ambient air
c_2 = speed of sound behind the preceding shock wave
$\boldsymbol{E}$, $\boldsymbol{F}$, $\boldsymbol{G}$ = flux vectors
M_{p0} = projectile Mach number with respect to the ground, (U_p/c_0)
M_{p2} = relative projectile Mach number with respect to the flow behind the shock wave, $[(U_p - u_2)/c_2]$
M_s = shock Mach number, (U_p/c_0)
$\boldsymbol{Q}$ = vector for conservative variables
$\boldsymbol{Q}_f$ = fortified solution; see Eqs. (2)
S_b = base area
$\boldsymbol{S}_v$ = viscous flux vectors
U_p = velocity of the projectile
U_s = speed of the preceding shock wave
u_2 = flow velocity behind the shock wave
χ = switching parameter; see Eqs. (2)
ϕ = circumferential angle, deg; see Fig. 6

Introduction

WHEN a projectile overtakes a preceding shock wave from behind, complex shock wave interaction occurs in the flowfield around the projectile. The projectile experiences a rapid variation of aerodynamic forces as it goes through the shock wave from the high-pressure region to the low-pressure region. The rapid change of aerodynamic forces may make the trajectory of the projectile unstable after the projectile overtakes the preceding shock wave. Such a flowfield is observed near the outlet of a ballistic range facility when the launched projectile overtakes the preformed blast wave (Fig. 1). Here, improvement of shot precision is needed for experiment accuracy. The same type of flowfield is also observed near the muzzle, where many experiments and theoretical studies have been carried out in the past.[1,2] However, most of the studies pursued the investigation of the flowfield over practical configurations, and there has been little discussion on the fundamental phenomena observed in such flowfields. An experimental study is difficult because of the short duration time of the phenomenon. Estimating aerodynamic forces is also difficult in experiments. Thus, numerical simulations are suitable for research of such flowfields.

The present authors carried out flow simulations based on the two-dimensional Euler equations and showed some fundamental flow features peculiar to overtaking the shock wave.[3] One of the most interesting features of such shock overtaking flows is that the flowfields are classified into two cases, supersonic overtaking and subsonic overtaking, according to the velocity difference between the projectile and the preceding shock wave. These two cases were considered, and the difference of the computed flowfields was discussed. The viscous flow computation[4] was also carried out around a blunt-based projectile by solving the two-dimensional, thin-layer Navier–Stokes equations to clarify the interaction between the shock wave and the wake flow. Computed results showed that the flowfield of the subsonic overtaking case is more complicated than that of the supersonic overtaking case because the preceding shock wave intensely interacts with the asymmetric wake vortex street when the projectile base passes through the shock wave. Although the fundamental flow characteristics were clarified by the two-dimensional flow computations, the flowfield obtained may be different in three dimensions because the shape of a launched projectile is cylindrical. Thus, further investigation is necessary, based on the three-dimensional flow computation. In the present paper, three-dimensional flowfields around the projectile overtaking the preceding shock wave are considered, and the transient shock interaction fields are investigated by solving the unsteady Navier–Stokes equations. The aerodynamic forces acting on the projectile are also investigated.

To supply reasonable grid configurations for such flowfields, the zonal grid approach, combined with the fortified solution algorithm (FSA),[5] is used. A local fine grid is prepared around the projectile in addition to the global grid, which covers the whole computational region. In addition, a relatively fine grid is prepared to adequately capture the shock/shock interactions and the shock/vortex interactions near the projectile.

Received May 16, 1997; revision received May 29, 1998; accepted for publication June 8, 1998.

*Graduate Student, Department of Mechanical Systems Engineering; currently Research Associate, Department of Mechanical Systems Engineering, Musashi Institute of Technology, 1-28-1, Tamazutsumi, Setagaya, Tokyo 158-8557, Japan. Student Member AIAA.

†Professor, High Speed Aerodynamics Division, Yoshinodai 3-1-1, Sagamihara. Associate Fellow AIAA.

‡Professor, Department of Mechanical Systems Engineering, Nakacho 2-24-16, Koganei.

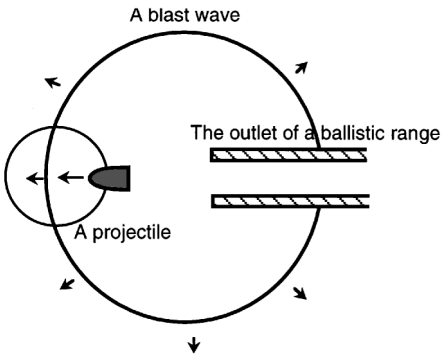

Fig. 1 Flowfield around the outlet of a ballistic range.

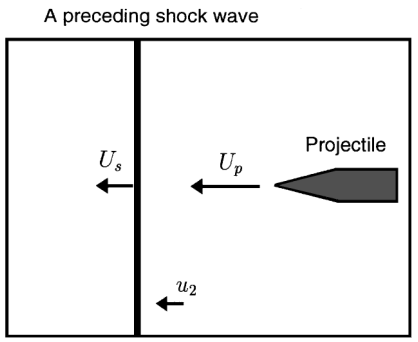

Fig. 2 Schematic of the flowfield.

Flowfield

Figure 2 shows the schematic of the simulated flowfield. It consists of a propagating normal shock wave and a moving projectile. The projectile, which moves faster than the preceding shock wave, overtakes it from behind. As the projectile moves in the velocity field induced by the preceding shock wave u_2, the projectile speed relative to the flow behind the preceding shock wave may become either supersonic or subsonic, although the projectile moves at supersonic speed relative to the ground. The flowfields are classified into two cases according to the velocity difference between the projectile and the preceding shock wave.

Supersonic Overtaking

The velocity relations are plotted in Fig. 3 in terms of the Mach numbers. Here, the abscissa indicates the shock Mach number M_s, and the ordinate indicates the projectile Mach number with respect to the ground M_{p0}. The relative projectile Mach number with respect to the flow behind the shock wave M_{p2} can be calculated using the normal shock relations. When the projectile speed is much higher than the preceding shock speed, M_{p2} is supersonic. We call this situation supersonic overtaking. It occurs in the region above the dashed line in Fig. 3. The dashed line indicates the case in which M_{p2} becomes unity.

Subsonic Overtaking

The case in which M_{p2} becomes subsonic is called subsonic overtaking, and it occurs in the region between the solid and dashed lines. The solid line indicates the case in which the shock wave and the projectile move at the same speed. In the region bellow the solid line, the projectile never overtakes the preceding shock wave, and it is not of interest here. The flow Mach number around the projectile suddenly increases when the projectile passes through the preceding shock wave because the projectile becomes free from the velocity reduction effect due to the shock-induced flow. In the case of supersonic overtaking, the Mach number changes from lower supersonic to higher supersonic, whereas it changes from subsonic to supersonic in the case of subsonic overtaking.

These two cases were investigated in the two-dimensional flow computations,[3,4] and it was found that the aerodynamic forces vary more than those for the supersonic overtaking case. Because our final interest is focused on the projectile behavior, we focus on the subsonic overtaking case in the present three-dimensional flow computation.

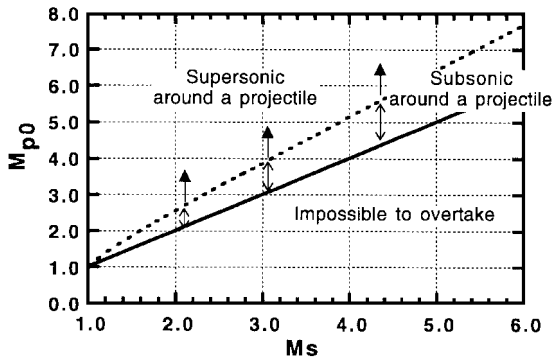

Fig. 3 Mach number relations behind the preceding shock wave.

Numerical Method

The basic equations are the unsteady three-dimensional, thin-layer Navier–Stokes equations written in the generalized coordinate system:

$$\partial_t \hat{\boldsymbol{Q}} + \partial_\xi \hat{\boldsymbol{E}} + \partial_\eta \hat{\boldsymbol{F}} + \partial_\zeta \hat{\boldsymbol{G}} = Re^{-1} \partial_\zeta \hat{\boldsymbol{S}}_v \tag{1}$$

A domain decomposition method with the FSA interface scheme is used to resolve the unsteady interaction between the projectile and the preceding shock wave. The FSA is an interface scheme to transfer physical data between zonal grids. When the FSA is applied to the basic equations, they are rewritten as

$$\partial_t \hat{\boldsymbol{Q}} + \partial_\xi \hat{\boldsymbol{E}} + \partial_\eta \hat{\boldsymbol{F}} + \partial_\zeta \hat{\boldsymbol{G}} = Re^{-1} \partial_\zeta \hat{\boldsymbol{S}}_v + \chi(\hat{\boldsymbol{Q}}_f - \hat{\boldsymbol{Q}}) \tag{2}$$

The fortifying solution $\hat{\boldsymbol{Q}}_f$ is added as the forcing terms to the right-hand side with the switching parameter χ. When χ is sufficiently large, the solution is fortified to be $\hat{\boldsymbol{Q}}_f$, in other words, $\hat{\boldsymbol{Q}}^{n+1} = \hat{\boldsymbol{Q}}_f$. When χ is zero, the equations go back to the original Eqs. (1). Thus, we can overlay the fortifying solution $\hat{\boldsymbol{Q}}_f$ onto the solution $\hat{\boldsymbol{Q}}$ by setting the χ parameter to be large in the appropriate region. The solution obtained with the finer grids or the other zones having higher priority is implemented on $\hat{\boldsymbol{Q}}_f$. Modification to the lower–upper alternating direction implicit factorization time-integration algorithm[6] that is used in the present computation and further descriptions are given in Ref. 5.

The convective terms are discretized with Roe's flux difference splitting, and higher-order space accuracy is obtained using MUSCL, the primitive variable interpolation.[7] The viscous terms are evaluated by central differencing, and the eddy viscosity is modeled by the Baldwin–Lomax turbulence model.[8]

Computational Grids

Figure 4 shows the zonal grid arrangement used. The computational domain is divided into three zones: the zone around the projectile, the global zone, and the intermediate zone. The projectile grid resolves the boundary layer attached to the projectile surface and the unsteady shock/boundary layer interaction observed during the overtaking. The intermediate zone is introduced for capturing the unsteady shock wave interactions observed around the projectile throughout the overtaking. Another important function of the intermediate zone is to reduce the interpolation errors due to the large difference of the grid size between the global and the projectile grids. The numbers of the grid points are $[126(\xi) \times 55(\eta) \times 35(\zeta)]$ for the projectile grid, $(111 \times 55 \times 51)$ for the intermediate grid, and $(62 \times 43 \times 45)$ for the global grid. The total number of the grid points is 673,875. In the present computation, viscous effects are only taken into account in the projectile zone with the thin-layer approximation. Euler equations are used in the other zones.

The details of the projectile grids are shown in Fig. 5. The coordinate system and the notations are given in Fig. 6. An axisymmetric

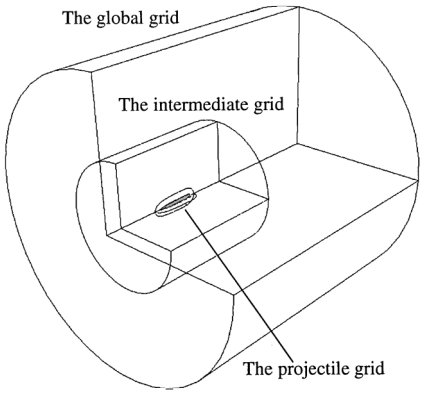

Fig. 4 Zonal grid arrangement.

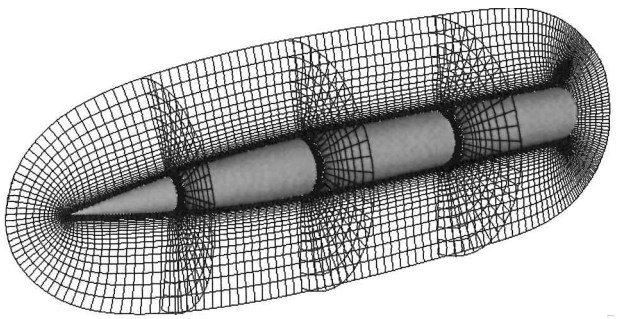

Fig. 5 Grid distribution around the projectile.

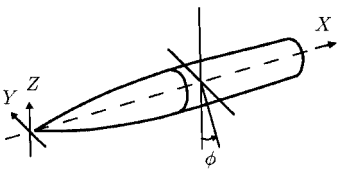

Fig. 6 Coordinate system and notations.

blunt-based projectile, which has an ogive cylinder configuration, is considered to clarify the interaction between the shock wave and the wake flowfield. The chord length of the projectile is taken to be 1.0, and the diameter of the base is 0.1. The O–O-type grids are distributed around the projectile by the hyperbolic grid generation method. The minimum spacing at the wall is 2.0×10^{-5} in the normal ζ direction, which is sufficient for capturing the turbulent boundary layer. (The Reynolds number is set to be 1.0×10^5 based on the projectile diameter.) The H–O-type grids are distributed for the intermediate and the global zones by the algebraic grid generation method. The whole computational region of the global zone ranges from -1.5 to 5.0 in the x direction and from -10.0 to 10.0 in the y and z directions. The leading edge of the projectile is taken to be the origin of the coordinates fixed to the projectile.

Calculation Procedure

In the case of subsonic overtaking, the unsteady flow computation should be started with the initial projectile location far enough from the preceding shock wave because the perturbation of the projectile propagates to the front and the preceding shock wave is influenced by the projectile as it approaches the shock wave. However, it would require enormous computer time. Thus, the steady flow computation is carried out in advance to set up an approximate initial solution for the following unsteady computation. The unsteady flow computation starts with the preceding shock wave located 1.0 in front of the projectile.

A no-slip wall condition is used on the projectile wall. All physical variables are extrapolated at all of the boundaries of the global grid except the inflow boundary, where its conditions are fixed to the state of the uniform supersonic flow.

Computed Results

The flow conditions are as follows: The Mach number of the preceding shock wave M_s is 1.5. For this shock Mach number, subsonic overtaking occurs when the projectile Mach number with respect to ground M_{p0} is less than 1.84. M_{p0} is taken to be 1.7 in the present case, and the relative projectile Mach number with respect to the flow behind the shock wave M_{p2} becomes subsonic ($=0.87$). The integration time step is 2.0×10^{-4} in nondimensional time so that the unsteadiness of the flowfield is properly captured.

Figures 7a–7e show a series of density contour plots on the cross section $y = 0$. Figure 7a shows the initial state of the unsteady flow computation ($t = 0.00$). Because the flowfield around the projectile is subsonic until the projectile overtakes the preceding shock wave, the typical subsonic flow features, such as the asymmetric wake flow, are observed. When the projectile overtakes the preceding shock wave, it starts coming out to the still air, and then the conical shock wave is generated from the nose (Fig. 7b; $t = 7.05$). Both the subsonic and supersonic flowfields are observed across the preceding shock wave. Namely, the flowfield around the projectile changes from subsonic to supersonic during the overtaking process. As already mentioned, this transition is observed only in the case of subsonic overtaking, and the flowfield is distinguished from other shock/projectile interactions. Another interesting observation in Fig. 7 is that boundary-layer separation occurs on the surface, where the foot of the preceding shock wave is attached. This boundary-layer separation was not observed in the two-dimensional subsonic overtaking cases.[3,4] To show the difference clearly, the

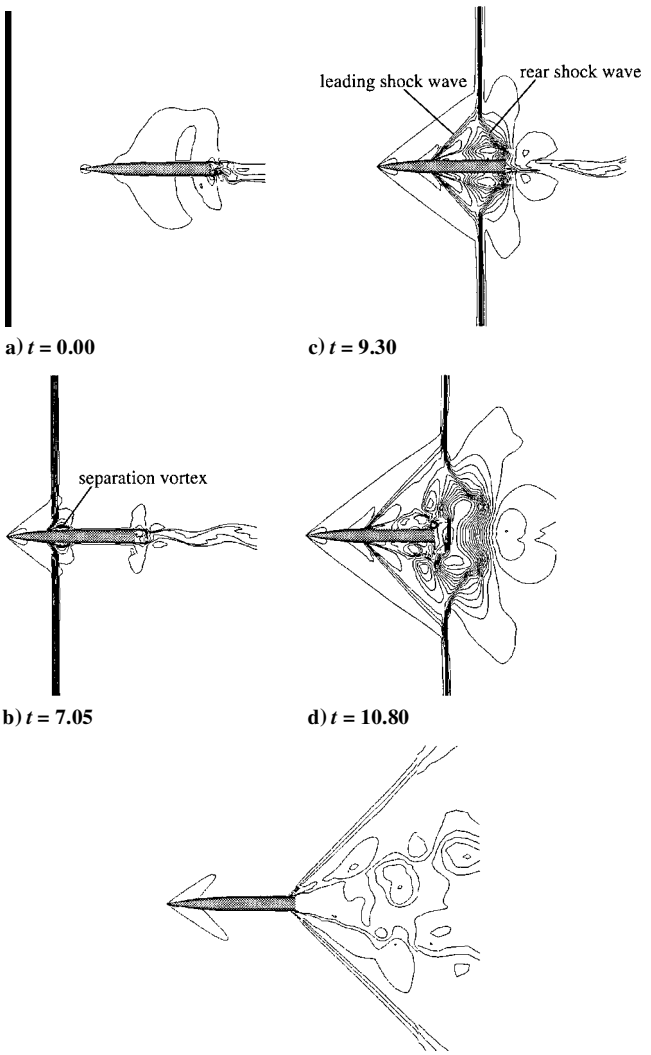

Fig. 7 Density contour plots around the projectile: $y = 0$.

density contours of the two-dimensional flowfield are plotted in Fig. 8. Comparing the contour plots in Fig. 8 with Fig. 7b, it is found that the degree of the shock/shock interaction is stronger in the two-dimensional flowfield. The difference is because two different types of nose shock waves are formed. In the two-dimensional flowfield, the nose shock is the oblique (plane) shock wave, whereas it is the conical shock wave in the three-dimensional flowfield. Because the shock strength of the conical shock wave is weaker than that of the oblique shock wave, the pressure rise across the nose shock wave is lower in the three-dimensional case, as seen in the plot of the surface pressure comparison (Fig. 9). In addition, the pressure behind the preceding shock wave in the three-dimensional case is higher than in the two-dimensional case because the flow expansion along the three-dimensional body is weaker than in the two-dimensional case. As a consequence, the projectile surface experiences the high adverse pressure gradient in the three-dimensional flowfield seen in Fig. 9. The pressure ratio across the preceding shock wave on the projectile surface is about 7 in this C_p plot, which is 2.2 in the pressure. Although experimental evidence is required for the existence of the boundary-layer separation, it may occur under such a high adverse pressure gradient. The separation region develops as time passes. In Fig. 7c ($t = 9.30$), it is observed that the preceding shock wave is bifurcated due to the flow separation. Around time $t = 9.4$, the projectile base passes through the rear foot of the preceding shock wave, as shown in Fig. 7d ($t = 10.80$). At this time, the flowfield around the base is disturbed by the interaction between the overtaken vortex ring and the projectile base, and the flow asymmetry appears. Similar asymmetry is also observed on the other section $z = 0$, as shown in Fig. 10 ($t = 10.80$).

Because such an asymmetric flowfield induces the asymmetric forces on the projectile body, it is important to understand the detail of the interaction flowfield. Figures 11a–11c show magnified views near the base around the time when the interaction occurs. In Fig. 11a, the projectile base is passing through the rear shock wave and begins to interact with the separation vortex attached to the foot. Once the base has overtaken the separation vortex, another counter-rotating vortex is formed at the base corners, as seen in Fig. 11b. To help understand the formation process of the interaction flowfield, the schematic of the flowfield is shown in Fig. 12, and velocity vectors relative to the speed of the projectile on the cross section $y = 0$ are plotted in Fig. 13. The vortex ring induces the strong reverse flow toward the base wall, as seen in Fig. 13, and the flow impinges on the base wall. As a result, the impinging shock wave is formed

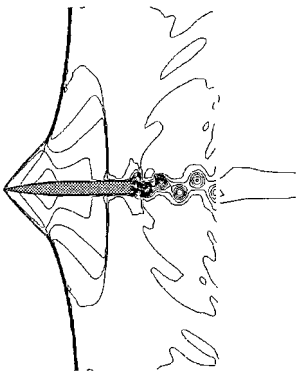

Fig. 8 Result of two-dimensional flow computation (density contours).

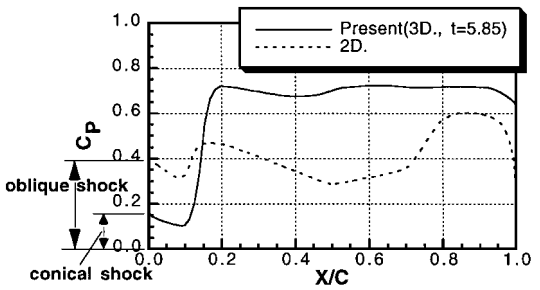

Fig. 9 Comparison of the C_p distributions.

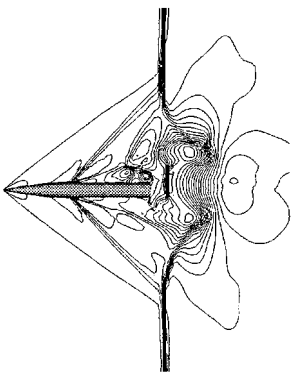

Fig. 10 Density contours on the cross section $z = 0$, $t = 10.80$.

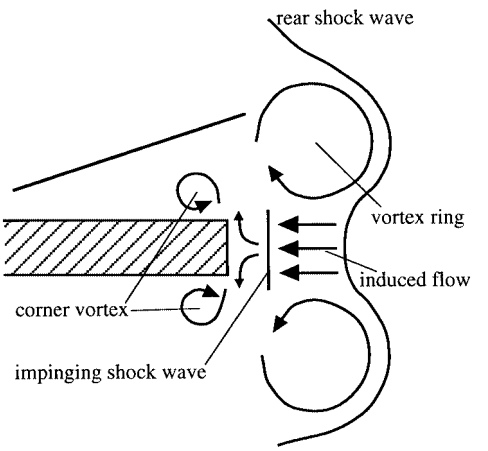

Fig. 12 Schematic of the interaction flowfield.

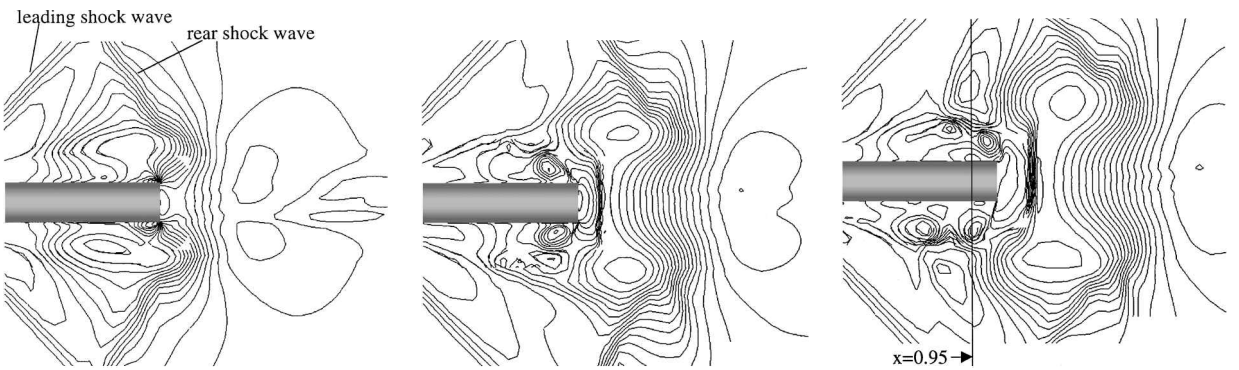

a) $t = 9.75$ **b) $t = 10.50$** **c) $t = 10.80$**

Fig. 11 Magnified views near the base; density contours on $y = 0$.

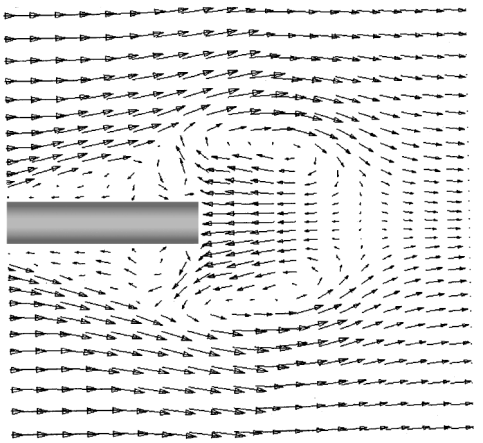

Fig. 13 Velocity vectors on the cross section $y = 0$, $t = 10.50$.

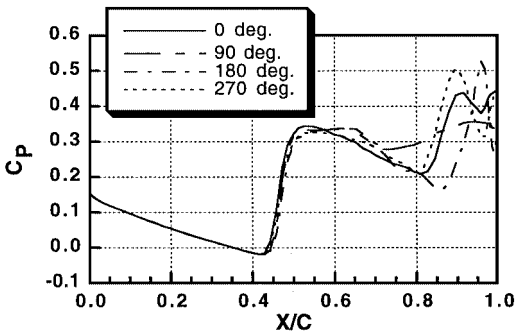

Fig. 14 Comparison of the C_p distributions, $t = 10.80$.

between the base and the vortex ring. The direction of the induced flow is turned at the base wall toward the base corners, and then the corner vortex is formed due to the separation at the corners. The degree of the flow asymmetry is amplified by the interaction and the instability of the vortex ring itself. Thus, the flowfield around the base becomes highly asymmetric, as shown in Fig. 11c. The asymmetric flowfield causes the pressure difference on the projectile surface near the tail, and it is observed in Fig. 14. It shows the pressure distributions along the four radial locations on the body surface. Large moment forces may be induced around the projectile as the asymmetric forces occur near the tail.

Considering that the apparent flowfield asymmetry was not observed in the supersonic overtaking case (not shown here), it seems that the flowfield asymmetry observed here comes from the wake flow asymmetry and the interaction between the separation vortex and the projectile base. Although there are some numerical sources for the asymmetry (the factorization errors of the implicit time integration, the small asymmetry of the metrics or the Jacobians), the computed flowfield becomes asymmetric, which is proper as a physical solution.

After overtaking the preceding shock wave, the projectile moves in the atmospheric air with supersonic speed followed by the axisymmetric wake. However, it takes a long time before the complete supersonic flowfield is established because the flowfield around the rear portion of the projectile is disturbed by the interaction flowfield (see Fig. 7e; $t = 22.75$).

Aerodynamic Force Histories

Because our interest is focused on the projectile behavior during overtaking, it is important to analyze the time history of the aerodynamic forces acting on the projectile. Figure 15a is the time history of the x-component force nondimensionalized by the base area. The drag force is almost constant until the projectile reaches the preceding shock wave, and it starts decreasing at that time. The rapid reduction of the drag force is the distinctive feature of the flowfield observed when the projectile overtakes the shock wave from behind. It is due to the pressure drop on the part of the projectile that has

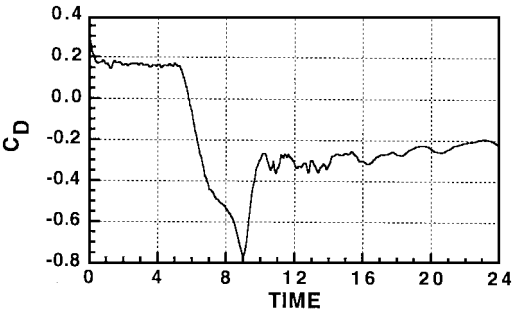

a) x Component force

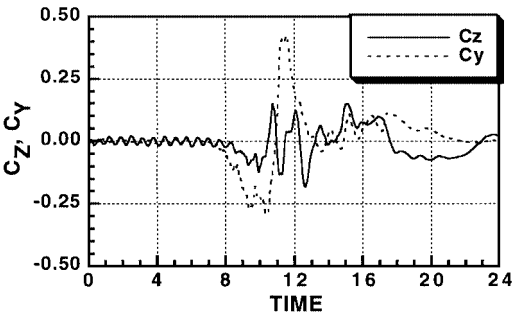

b) Lateral forces (z and y components)

Fig. 15 Time histories of the aerodynamic force components.

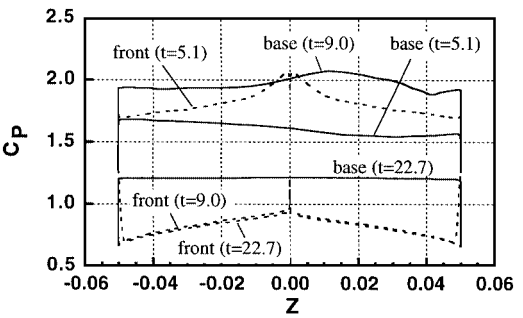

Fig. 16 Variation of the C_p distribution.

overtaken the preceding shock wave. Figure 16 shows the variations of the pressure distributions along the base and the front portion of the projectile. The negative C_D value after $t = 6.0$ comes from the inversion of the pressure level between the base and the front portion. This state continues until the projectile becomes free from the flowfield disturbed by the interaction with the preceding shock wave. However, the projectile base is still under the influence even though it goes far forward (Fig. 7e; $t = 22.75$), and the base pressure is higher than that of the front portion (Fig. 16). Thus, the C_D value is still negative at this time. However, it should become positive if we continue the computation further, and the complete supersonic flow is established around the projectile. The steady flow computation under the condition that the projectile is in uniform supersonic flow ($M_\infty = 1.7$) indicates that the asymptotic C_D value is 0.34. Further computation is not carried out because of the insufficient computational domain. Also note that the resultant aerodynamic force coefficients might be different from those obtained in a realistic firing test because no velocity/attitude change of the projectile is presently considered. However, it is reliable that the drag force shows a rapid decrease during the overtaking. The negative drag and the acceleration due to this may occur depending on the velocity relations, but its influence on the projectile trajectory may be small because the real time is very short. The nondimensional time $t = 24$ corresponds to $t = 6.9$ ms if we assume the projectile length to be 10 cm.

Figure 15b is the time history of the lateral forces (z and y components) nondimensionalized by the base area. The C_z, which is plotted as the solid line, starts decreasing when the base of the projectile

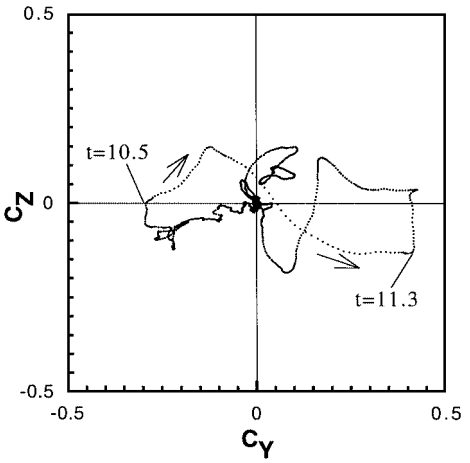

Fig. 17 Correlation between C_y and C_z.

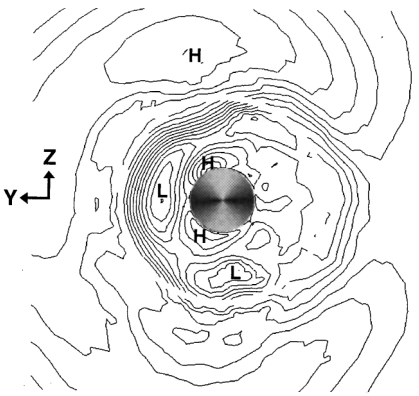

Fig. 18 Density contours on the cross section $x = 0.95$, $t = 10.80$.

passes through the separation vortex ($t = 8.0$) and shows the periodical variations after time $t = 10.0$. On the other hand, the history of C_y, which is plotted as the broken line, shows only the rapid decrease at $t = 8.0$ and the rapid increase at $t = 10.5$. The difference between these two force components comes from three dimensionality of the flowfield around the tail.

To understand the behavior of the forces on the $x =$ const. plane, the correlation between C_y and C_z is plotted in Fig. 17. This scatter plot shows the time variation of the direction and the magnitude of the aerodynamic force. Because the points are plotted in the same time intervals, the coarser distribution of the points means faster variation. The distance from the origin to the point is the strength of the force acting on the projectile. The rate of variation is largest when it moves from the second quadrant to the fourth quadrant, which corresponds to the time about $t = 11$. Further, the strength of the force shows a maximum value at $t = 11.3$. The reason the y component becomes larger than the z component is that the flowfield on the cross section $z = 0$ is more asymmetric (see Figs. 7d and 10). This flowfield asymmetry can be clearly seen in the density contour plot on the cross section $x = 0.95$ (Fig. 18; $t = 10.80$). The location of the section is indicated as the solid line in Fig. 11c. The high-density (pressure) regions appear on the upper and lower surfaces, whereas there is only the low-density region on the $+y$ side of the projectile.

For more detailed analysis of the projectile behavior, it is important to investigate the history of the moment forces. Figure 19 shows the time histories of the moment force components around the z and y axes. They are nondimensionalized by the base area and the chord length. The origin of the moment forces is taken to be the leading edge of the projectile. The C_{my} (solid line) and C_{mz} (broken line) show the same behavior as C_z and C_y respectively. The positive C_z causes the negative C_{my}, which heads downward, and the positive C_y causes the positive C_{mz} as the forces act on the rear portion. These moment force variations are also due to the interaction between the vortex ring and the projectile base as shown earlier. Periodical structure exists in the wake even before the overtaking, as can be seen in Fig. 7b. The periodic variation of the moment forces that occur due to this can be seen as a variation before $t = 8.0$ in Fig. 19. It is clear that the strength of the moment forces for the overtaking is an order of magnitude larger.

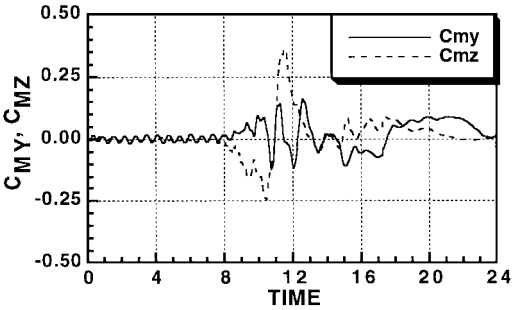

Fig. 19 Time histories of the moment force components.

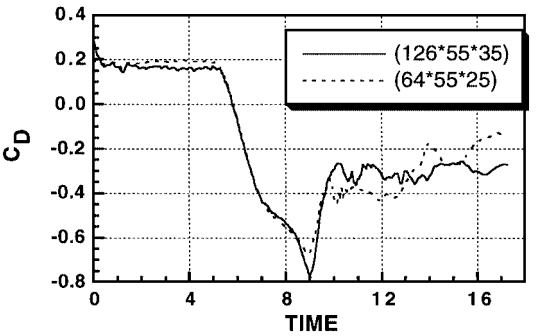

Fig. 20 Drag histories; effect of grid spacings.

Trajectory Estimation

The trajectory of the projectile can be estimated approximately by integrating the dimensionalized force/moment histories in time. Here, we assume the material of the projectile is steel (density $= 7.87 \times 10^3$ kg/m^3), and its length is 10 cm. Then, the mass of the projectile is 47.4 g. The estimated displacements in the y and z directions during the overtaking (about 5.0 ms) are -5.0×10^{-2} and -3.0×10^{-2} mm, respectively. It seems that the variation of the aerodynamic forces causes no significant contribution to the projectile trajectory. However, the deflection of the body axes due to the moment variation may create more displacement in a realistic situation. The estimated angular deflections around the y and z axes during the overtaking are $+1.0 \times 10^{-3}$ and $+1.2 \times 10^{-3}$ rad, respectively. Also note that the rate of the moment variation is very fast, i.e., the angular velocity becomes large. The maximum value of the angular velocity during the overtaking is 0.8 rad/s in the present computation.

Effects of Grid Spacings

To check the accuracy of the computed results, the effects of the grid spacing are investigated by changing the grid spacings of the projectile grid. The number of grid points of the projectile grid is reduced from $(126 \times 55 \times 35)$ to $(64 \times 55 \times 25)$, and the minimum spacing on the projectile surface is changed from 2.0×10^{-5} to 5.0×10^{-5}. Figure 20 shows the comparison of the drag force histories. Although some discrepancy (up to 30%) is observed after the base has overtaken the separation vortex at $t = 9.0$, the reduction of the grid points has no effect on the qualitative behavior of the drag force history. The present computation has sufficient accuracy to clarify the fundamental flow characteristics observed in the shock overtaking flowfield, which is the purpose of the present paper.

Conclusion

Numerical simulations of the flowfield around the projectile overtaking the preceding shock wave are carried out by solving the three-dimensional, thin-layer Navier–Stokes equations. The subsonic overtaking case is examined. The computed results show the

transition of the flowfield from subsonic to supersonic, which is the inherent nature of subsonic overtaking. The differences between the three- and two-dimensional flow computations are shown. The most distinctive phenomena are that there exists a strong adverse pressure gradient in the three-dimensional case and the boundary-layer separation is observed. The configuration and the formation of the interaction flowfield between the overtaken vortex ring and the projectile base are clarified. From the time histories of the aerodynamic forces, it is found that the projectile suffers strong asymmetric forces during the overtaking due to the interaction. The results indicate that the projectile path trajectory may be strongly disturbed during the overtaking.

References

[1]Schmidt, E. M., and Shear, D. D., "Optical Measurements of Muzzle Blast," *AIAA Journal*, Vol. 13, No. 8, 1975, pp. 1086–1091.

[2]Erdos, J. I., and Del Gudice, P. D., "Calculation of Muzzle Blast Flowfields," *AIAA Journal*, Vol. 13, No. 8, 1975, pp. 1048–1055.

[3]Watanabe, R., Fujii, K., and Higashino, F., "Numerical Simulation of the Flow Around a Projectile Passing Through a Shock Wave," AIAA Paper 95-1790, June 1995.

[4]Watanabe, R., Fujii, K., and Higashino, F., "Viscous Flow Computations of the Unsteady Flow Around a Projectile Overtaking a Preceding Shock Wave," *Proceedings of the 9th Japanese CFD Symposium*, Japan Society of Computational Fluid Dynamics, Tokyo, Japan, 1995, pp. 247, 248 (in Japanese).

[5]Fujii, K., "Unified Zonal Method Based on the Fortified Solution Algorithm," *Journal of Computational Physics*, Vol. 118, No. 1, 1995, pp. 92–108.

[6]Obayashi, S., Matsushima, K., Fujii, K., and Kuwahara, K., "Improvement in Efficiency and Reliability for Navier–Stokes Computations Using the LU-ADI Factorization Algorithm," AIAA Paper 86-0338, Jan. 1986.

[7]Fujii, K., and Obayashi, S., "High-Resolution Upwind Schemes for Vortical Flow Simulations," *Journal of Aircraft*, Vol. 26, No. 12, 1989, pp. 1123–1129.

[8]Baldwin, B. S., and Lomax, H., "Thin-Layer Approximation and Algebraic Model for Separated Turbulent Flows," AIAA Paper 78-257, Jan. 1978.

T. C. Lin
Associate Editor